ASEAN Engineering Journal

Full Paper

DEVELOPMENT OF DIRECT-INK WRITER FOR PROTOTYPING PAPER BASED CAPACITIVE SWITCH AND CHARACTERISATIONS

Thim Jia Ying[a], Chin Fhong Soon[a,b*], Nabilah Ismeran[b,e], Norhidayah Che Ani[b], Faezahana Mohkhter[b], Farshid Sefat[c], Suhana Mohamed Sultan[d], Kian Sek Tee[a]

[a]Faculty of Electrical and Electronic Engineering, Universiti Tun Hussein Onn Malaysia, 86400 Batu Pahat, Johor, Malaysia.
[b]Microelectronics and Nanotechnology–Shamsuddin Research Centre, Institute for Integrated Engineering, Universiti Tun Hussein Onn Malaysia, 86400 Parit Raja, Batu Pahat, Johor, Malaysia.
[C]Biomedical and Electronic Engineering Department, School of Engineering, University of Bradford, BD7 1DP Bradford, United Kingdom.
[d]School of Electrical Engineering, Faculty of Engineering, Universiti Teknologi Malaysia, 81310 UTM Johor Bahru, Johor, Malaysia.
[e]Nine G Solutions Sdn. Bhd. Level 10, Suite 1A, Perak Techno Trade Centre (PTTC), Off Jalan Jelapang, Bandar Meru Raya, 30020 Ipoh, Perak, Malaysia.

Article history
Received
23 June 2024
Received in revised form
12 December 2024
Accepted
14 February 2025
Published online
31 August 2025

*Corresponding author
soon@uthm.edu.my

Graphical abstract

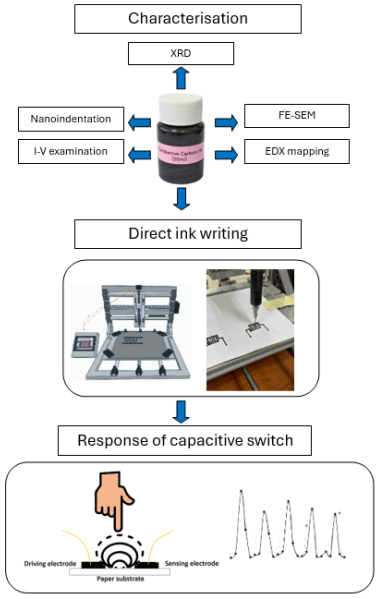

Abstract

This study presents a comprehensive investigation into the development and application of direct ink writing (DIW) techniques for rapid and cost-effective prototyping of capacitive switches. The research applied direct writing with mini-CNC and extrusion systems to achieve precise control over the carbon ink deposition process, enabling the fabrication of complex sensor geometries with high accuracy. The performance and characteristics of a fabricated capacitive sensor were evaluated using various characterization techniques, including Field Emission-Scanning Electron Microscopy (FE-SEM) for morphological examination, Energy Dispersive X-ray (EDX) for elemental mapping, Xray-diffraction (XRD) for assessing the crystallinity of the carbon composite material, nanoindentation for mechanical property assessment, and current-voltage and capacitance measurements. With 47.4% carbon content, as indicated by the FE-SEM, the printed carbon trace's elastic modulus and electrical conductivity are determined at 3.31±1.3 GPa and range from 100 to 190 S/m, respectively. The physical mixed carbon composite ink remains highly crystalline and robust as indicated by the XRD and EDX results. Nanoindentation suggested the need for a protective liner to avoid plastic deformation, but this altered the log ΔC of the capacitive switch. The printed capacitive switch is responsive to 3 to 4 Hz of tapping. The study demonstrates the application of DIW in printing functional capacitive switches with suitable physical and electrical properties, contributing to the realization of innovative and versatile sensor fabrication solutions.

Keywords: Graphite, Carbon Ink, Direct Ink Writing, Capacitive Sensor, Electronic Materials.

© 2025 Penerbit UTM Press. All rights reserved

1.0 INTRODUCTION

Planar capacitive switches have many applications in proximity, material characterization, and pressure sensing due to their simplicity, sensitivity, and versatility [1, 2, 3]. These switches can be used in various industries due to their contactless, wear-free, and lower power consumption. The components of a planar capacitive switch include two conducting bodies separated by a non-conducting material (dielectric), electrodes arrayed on the same plane, and a high-frequency oscillator integrated with two

sensing electrodes for capacitive proximity sensors [4]. There are two main electrode configurations used in capacitive proximity sensors: Dielectric Type (D-Type) and Conductive Type (L-Type) [5]. D-type sensors have two sensing electrodes integrated into an oscillator, detecting all materials. In contrast, L-type sensors use one sensing electrode and rely on a conductive material entering the field to oscillation [5]. The back-plane support can be polymer or cellulose paper, which functions as dielectric material in the device. The sensing distance of a planar capacitive switch depends on the material being sensed, with conductive materials allowing for greater sensing distances than dielectric materials [5].

However, planar switches are usually made of FR-4 board and copper, which is difficult to decompose and becomes electronic waste after the end-of-life cycle. Hence, the current work presents a prototyping method that creates an environmentally friendly electronic device. Paper-based devices have gained significant attention in recent years due to their versatility, low cost, and eco-friendly nature. The methods to produce paper-based devices include screen printing, inkjet printing, laser cutting, and direct ink writing. Screen printing is widely used for depositing conductive ink, such as silver and carbon-based inks, onto a paper substrate [6]. This method allows for intricate patterns and designs, making it suitable for fabricating electrodes, interconnects, and other functional components in large quantities. A large volume of waste was found using this technique. Inkjet printing is a digital printing technique that can deposit functional inks, including conductive, dielectric, and sensing materials, onto paper substrates [7]. This method offers high precision, flexibility, and the ability to create complex patterns and designs on paper. However, this technique requires particles of nanometric size, and clogging can be a potential problem. Laser sintering and etching techniques can be applied to pattern paper substrates, creating intricate designs and structures for paper-based sensors and devices [7]. This method allows for the fabrication of complex geometries and integrating various functional components [7]. One potential problem with using laser cutting and etching techniques on paper substrates is the fire risk. Paper is highly flammable, and the intense heat generated by lasers can ignite the paper if not adequately controlled.

Direct Ink Writing (DIW) is a versatile additive manufacturing technique that allows for the rapid prototyping of capacitive devices cost-effectively [8]. In addition, DIW enables the fabrication of intricate and complex capacitive switch designs, offering a high degree of customization and design flexibility. Another advantage of the DIW process is that it simplifies the manufacturing of devices, as it involves the extrusion of uncured ink or gel material rather than relying on temperature-dependent printability. The rheological properties of the DIW inks can be optimized to ensure good shape fidelity and stability of the printed capacitive switch structures, leading to enhanced performance and reliability [9]. Capacitive switches are pivotal in human-computer interaction, facilitating interaction with various electronic devices. This research paper presents the intricate process of utilizing DIW to prototype D-type capacitive switches on paper, focusing on the fabrication and characterization aspects. The benefits of using paper-based sensors are affordability, simplicity in manufacturing, ease of operation, portability, and disposable nature. By exploring the intricate interplay between material properties and capacitive responses, this study aims to comprehensively apply DIW to create efficient and reliable capacitive switch prototypes on paper substrates.

A series of characterization techniques have been employed to evaluate the performance and characteristics of the fabricated capacitive sensor. These include Field Emission Scanning Electron Microscopy (FE-SEM) for morphological examination, Energy Dispersive X-ray Spectroscopy (EDX) for elemental analysis, nanoindentation for mechanical property assessment, current-voltage measurement and capacitance measurement for evaluating the sensor's sensing capabilities. The capacitive sensor's switching and capacitive characteristics were characterized using a microcontroller circuit and a capacitance measurement meter. This research elucidates the capacitive sensor's structural, mechanical, and electrical properties through these multi-dimensional characterization approaches. It provides insights into its potential applications in fields such as wearable switches.

2.0 MATERIALS AND METHOD

A direct-ink writer based on computer number control (CNC) was developed, as shown in Figure 1. The CNC machine has a robust frame, linear motion systems, a printhead mounting system, and a control unit. The direct ink printer combines a CNC system's precise motion control with an extruder's material deposition capabilities. The printhead of the CNC machine is modified to accommodate the extrusion mechanism required for direct printing. The printhead involves the installation of a syringe-based extruder capable of depositing carbon ink onto the substrate with high precision.

The system employs the ZK-SMC02 CNC Stepper Motor Driver to design the controller unit. This driver incorporates a user interface, such as a liquid crystal display (LCD), indicators, and clockwise (CW) and counterclockwise (CCW) buttons for the adjustment of rotation direction and speed of the stepper motor. The CW and CCW buttons control the infusion and diffusion of the extruder, respectively. Additionally, a potentiometer allows fine rotation speed adjustment in a range of 1 to 100 rotations per minute (RPM), while an LCD flow rate allows user selection. A 12V DC power source supplies power for the microcontroller and the stepper motor. The ZK-SMC02 CNC Stepper Motor attached to the extruder sends the pulse signals via A+, A-, B+, and B- wires to the stepper motor, thus providing precise and reliable control over a stroke length of 10 cm.

The syringe holder constitutes a pivotal component within the direct printer setup, providing essential functionality for containing and dispensing carbon ink onto the substrate during printing. The plunger holder was designed using Google SketchUp and produced by a 3D printer, as shown in Figure 1b. The syringe holder is attached to the printer's extruder system. At the same time, the plunger is pushed by the extruder in forward and reverse directions to produce the mechanism of infusion and diffusion of carbon ink, respectively. The syringe holder maintains the syringe's position, allowing for precise control over the deposition of ink or paste onto the paper substrate.

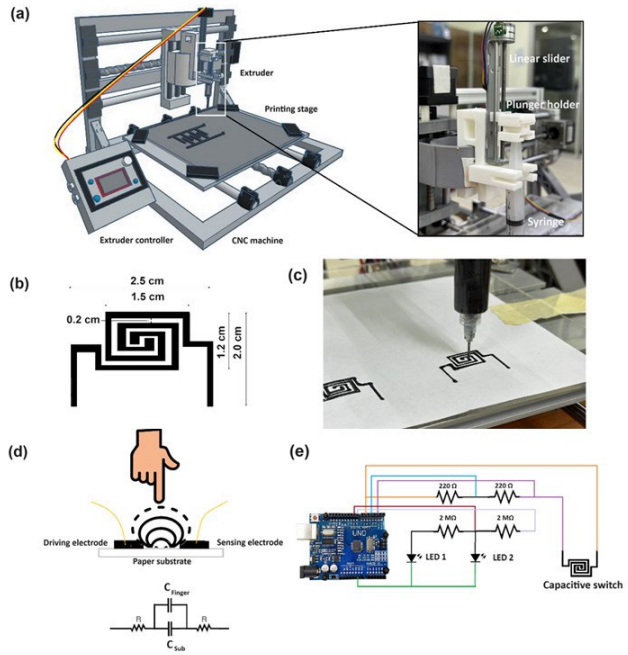

Figure 1 (a) The development of a direct ink writer and (b) The pattern of the winding capacitive switch, (c) directing writing of the carbon capacitive switch, (d) R-C model of the finger tapping on the capacitive sensor, and (e) Arduino microcontroller circuit used to measure the time responses of the capacitive switch in response to finger tapping.

The drawing pattern of the winding capacitive switch was produced using Inkscape software. As shown in Figure 1b, the planar capacitive sensor comprises two identical winding electrodes with a width of 1 mm separated by a short spacing of 1 mm. Then, the designed pattern in support vector graph format was converted into *ngc format, which is readable by the controller of the CNC machine. Paper is the dielectric material between the two electrodes used to form the base capacitor (C_{sub}). The pattern was plotted with conductive carbon ink using the DIW developed. The response time of the capacitive switching to finger tapping was measured using an Arduino-Uno microcontroller and R-C network circuit as shown in Figure 1c.

To prepare the carbon ink, 30 g of micronized graphite powder (Sigma Aldrich, UK) with a mesh size of 60 µm was measured and mixed into 10 ml of sodium silicate solution. The graphite powder was gradually poured into the sodium silicate solution while stirring continuously to ensure thorough mixing and dispersion of graphite particles. Once the desired concentration is achieved, the carbon ink is ready to be filled in a 5 ml syringe.

The capacitive characteristics of the paper-based planar capacitor were determined using an LCR189 meter. The planar capacitive sensor was connected to the LCR meter via probes. The LCR meter for the capacitance measurement was set to the C/R mode, with a bias voltage of 1.275V, and various frequencies were applied, ranging from 0.5 kHz to 10 kHz. The capacitance measurements with (ON state) and without (OFF state) finger tapping was repeated at least three times for each test frequency.

A linear line of conductive carbon ink with a length of 4 cm was printed on a paper substrate. The printed pattern was placed on a two-channel probing station and device test fixture that is connected to the source measurement unit of a semiconductor parametric analyzer (SPA, Keysight B1500A). Subsequently, the current-voltage (I-V) measurement of the conductive carbon printing was conducted at 1 to 4 cm using the SPA. The device was applied with a range of voltages from 0 to 2V at an interval of 50 mV, and then, the current was determined by the SPA. The conductivity was determined using the formula of R = (σL/A) where σ is the conductivity, L is the length, A is the area of measurements. All experiments were repeated three times in three independent points.

The surface structures of the conductive graphite ink were investigated using a field-emission scanning electron microscope (JSM-7600F, JEOL, Japan) equipped with an upper secondary electron detector. The paper substrate containing the printed graphite ink pattern was cut and pasted on the sample holder using carbon tape. The surface elements of graphite ink were investigated using an energy-dispersive X-ray spectrometer (Quantax espirit core with XFlash®, Bruker, USA).

An X-ray diffractometer (PANalytical Xpert PRO) was used to study the crystallographic structure of the graphite paste. The sample with a thickness of 500 µm was coated on a glass slide and dried at room temperature. This thickness is similar to the thickness of the capacitive switch printed with the DIW on a paper substrate. After the sample was placed on an X-ray diffractometer, the intensity of the diffracted X-rays was measured as a function of the diffraction angle to produce the XRD pattern. Subsequently, the sample was scanned in the 2θ range of 5–80 ° (Bragg angle) with a step size of 0.5°/min and a scan step of 0.5 s. The XRD measurements were performed using 40 kV and 40 mA XRD, generating CuKα radiation with a wavelength (λ) of 1.5406 Å. The data were acquired using PANalytical Xpert HighScore software. The XRD pattern provides information on the sample's crystallinity and preferred orientation.

The crystalline size of the peak was calculated using Scherrer's equation. Where Lc is nanoparticles crystalline size, K is the Scherrer constant, λ denotes the wavelength, and beta is the full width at half maximum (FWHM) [10].

$$L_c = \frac{K\lambda}{\beta \cos\theta} \quad (1)$$

The interplanar spacing of each peak was then calculated using Bragg's Law, where n is the order of the XRD peak. d_{hkl} is the lattice spacing, and θ is the X-ray beam's incidence angle concerning the crystal lattice planes [10].

$$d_{hkl} = \frac{\lambda}{2 \sin\theta} \quad (2)$$

From the interplanar value for each peak, lattice constant, a can be determined using the derivation of Bragg's Law for a specific crystallographic plane with Miller indices (hkl) [11].

$$a = d_{hkl} \times \sqrt{h^2 + k^2 + l^2} \quad (3)$$

A nano-indenter (Hysitron TI Premier, Bruker Minneapolis, MN), a Berkovich diamond tip, was applied to determine the hardness (H) and reduced elastic modulus (E_r) of the printed graphite ink. The specimen was mounted on a glass slide using glue. The Berkovich tip applied a loading force of 1000 µN at a rate of 100 µN/sec, followed by a 5-sec hold-time before unloading. The Bruker data analysis software recorded the maximum depth, loading force, derived indentation hardness, and reduced modulus. The stiffness was calculated by linear fitting the tangent to the unloading curve at the maximum load. A similar experiment was repeated five times at randomly selected indentation sites, and average values of the parameters were calculated.

The elastic modulus (E) was calculated using Equation (4) [12],

$$E_r = \frac{E}{1 - v^2} \tag{4}$$

where E_r is the reduced elastic modulus and v is the Poisson's ratio. The Poisson's ratio of graphite flakes is 0.27 [13].

The indentation creep percentage, $C_{ID,}$ in Equation 5 was calculated based on the change in indentation depth during the holding section, where the applied load remains constant for 5 seconds [14].

$$C_{ID} = \frac{h_1 - h_o}{h_o} \times 100 \tag{5}$$

where h_o and h_1 are the initial contact depths before and after the hold section with a constant loading force.

3.0 RESULTS AND DISCUSSION

A linear line of carbon ink was written on a paper substrate, and the I-V measurement for different lengths of the carbon ink was measured at various lengths, ranging from 1 to 4 cm, as shown in Figure 2. The I-V curve displays nonlinear behavior, gradually increasing current as voltage is applied. The shorter lengths exhibit higher current than longer lengths, possibly due to less resistance as current travels through the carbon ink, resulting in higher current flow. This can be attributed to the shorter path length of the electron. Moreover, electrons encounter less resistance as they travel through the carbon ink over a shorter distance, facilitating higher current flow. The standard deviation of the mean values of resistance measurement ranges from 8.66 to 12.77 Ω for R(1cm), 9.22 to 12.49 Ω for R(2cm), 10.07 to 14.14 Ω for R(3cm), and 28.09 to 44.69 Ω for R(4 cm), respectively. The standard deviation of the SD of mean conductivity measurement ranges from 3.3 to 6.29 S/m for σ(1cm), 2.38 to 8.03 S/m for σ(2cm), 1.34 to 4.21 S/m for σ(3cm), 3.55 to 3.91 S/m for for σ(4cm), respectively.

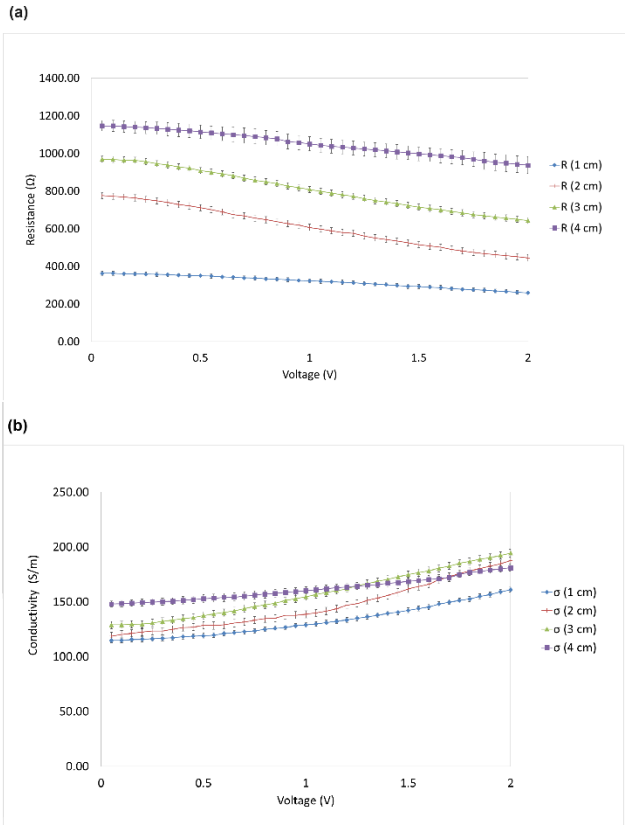

Figure 2 I-V measurement results for the carbon ink printed in line structure.

Further examination of the conductivity curve provides insight into the resistive characteristics of the carbon inks. As seen in Figure 2b, the conductivity increases with increasing voltage for all carbon ink lengths. This is due to the increased driving voltage potential force pushing the current through the carbon ink [15]. The conductivity computed ranges from 100 to 190 S/m for the applied voltage up to 2V. This range of conductivities displayed by the carbon ink is higher than the graphite-epoxy composite reported by [16]. This electrical conductivity is crucial for the functionality of sensors, as it enables the reliable and accurate detection of capacitance changes. Although the SD of resistance and conductivity for all four measurement lengths turned larger when the distances of measurements were increased, the SD percentage of resistance and electrical conductivity for each measurement length are still well within 5%.

The FE-SEM image of graphite ink (Figure 3a) shows that the morphology of the graphite ink is a needle-like structure with a length and width in the micro-size range. The structures have an almost uniform shape with practically no cluster formation. In Figure 3(b), the elemental EDX mapping for graphite ink is presented, revealing the presence of carbon (C), oxygen (O), sodium (Na), and silicon (Si). Further examination in Figure 3 (c and d) reveals detailed element mapping for areas 1 and 2, designated as Spectrum 1 and Spectrum 2, respectively. The elemental composition of these areas differs significantly. Area 1 displays compositional proportions of C 47.40%, O 32.16%, Na 2.33%, and Si 18.11%, whereas area 2 consists of C 12.95%, O 46.05%, Na 24.28%, and Si 16.72%. Figure 3(d) shows that area

1 contains a higher C concentration than area 2, while area 2 exhibits a higher Na content than area 1. This result shows that a small area contains more carbon. In contrast, another small area contains more sodium silicate than the carbon as indicated in the elemental mapping of a composite (Figure 3b and 3d).

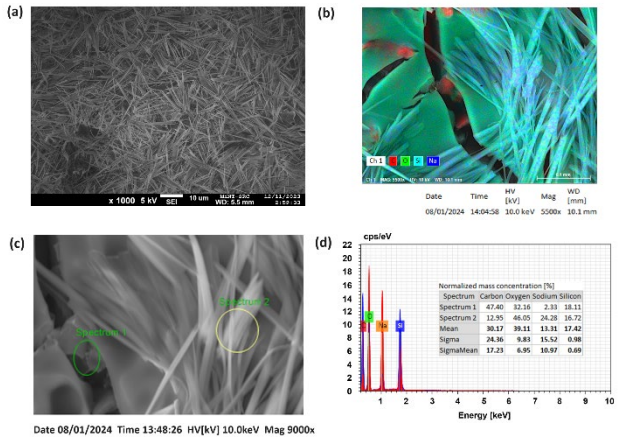

Figure 3 Photomicrograph of (a) FE-SEM of the graphite ink, (b) EDX mapping of the elements for graphite ink, and (c) location for Spectrum 1 and 2, (d) detailed element mapping for the areas 1 and 2 that are denoted as Spectrum 1 and 2, respectively

Figure 4 shows the X-ray diffraction of the graphite paste sample. When examining the crystalline structure of carbon materials, such as graphite, X-ray structural analysis is typically used to determine the degree of order in the structure and the size of the crystallites [17]. The two peaks of 2θ shown in Figure 4 were identified at 26.44 and 54.54˚ for the intensity reflexes (002) and (004), respectively. The reflexes represent the polyarene layers [18]. These two peaks were associated with the crystallographic size of the carbon.

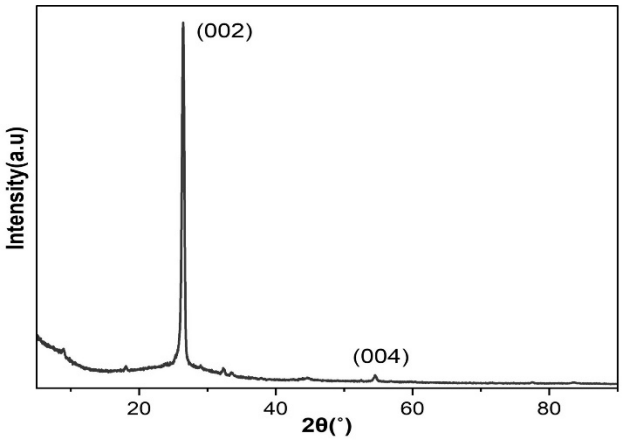

Figure 4 XRD pattern of the carbon ink reinforced with sodium silicate.

According to previous research [19], the XRD pattern for pure graphite is close to the baseline between 5˚ to the first peak at 26.44º. However, in the sample of this study, the presence of sodium silicate did not influence much of the XRD pattern. With the presence of the sodium silicate, a small diffraction peak was seen between 2θ angle of 5 to 12.12˚. This peak is an effect of amorphous silica [20]. At low 2θ angles, the XRD broadening peak is due to the large unit cell from sodium silicate [21].

Table 1 shows the parameters calculated for the XRD. It is obvious how the size of the crystallites affects the normalized diffraction intensity. Even though the XRD patterns were generated using identical lattice parameters, the full width at half maximum (FWHM) increases with decreasing crystallinity size [22]. The interplane distance, d_{hkl} is significantly less when compared with the graphite reported in a previous study [23].

Table 1. The calculated XRD parameters.

Estimate from reflex,	Full width at half maximum (FWHM)	Interplane distance, d_{hkl} (nm)	Lattice constant, a (Å)	Peak Crystallinity, L_c (nm)
(002)	0.464	3.367	6.734	3.630
(004)	87.760	1.681	6.722	0.030

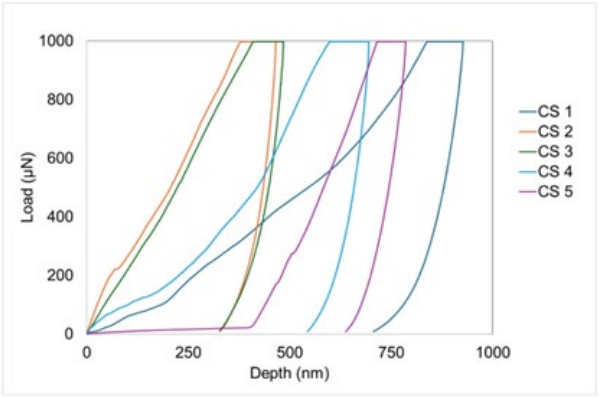

Figure 5. Load and unload displacement curves for the nanoindentation of the printed carbon ink.

Figure 5 shows the nanoindentation to the surface of the printed graphite ink. The indentation displacement was between 300 to 1000 nm under a peak loading force of 0.1 mN. The lower displacement indicates resistance to the indentation. The average E and CID were determined at 3.31±1.3 GPa and 19%, respectively. This composite material has displayed high hardness that could withstand force from finger tapping. The characteristic curves in Figure 5 are similar to the carbon nanotubes composite reported in [24]. Graphite ink is a composite material of micronized graphite flakes and sodium silicate. Hence, the loading and unloading parts of the nanoindentation curves involve nonlinearity induced by the nonlinear composite material behavior and the increasing contact area. Under a constant holding load, the load-displacement curve at the peak force characterized by creep displacement might be attributed to the typical plastic deformation of the carbon material [14]. Based on this behavior,

an acrylic adhesive tape as a liner was applied to protect the surface of the capacitive switch.

This technique utilizes a syringe pump device to directly deposit ink onto a paper substrate, enabling the creation of sensors with complex shapes that would be challenging to achieve using traditional manufacturing methods [25]. One of the critical advantages of DIW is its ability to deposit materials in a controlled manner, enabling the fabrication of sensors with intricate designs and geometries. Furthermore, this study highlights using carbon ink reinforced with sodium silicate as a suitable material for DIW. This work created a capacitive sensor that can accurately detect and measure the changes in captive signals, as shown in Figure 1. Since the nanoindentation results imply that the carbon ink is subjected to plastic deformation when pierced by a sharp indenter, the acrylic adhesive film was applied to protect the capacitive switch. This work also investigated the effects of applying acrylic adhesive liners to capacitive characteristics.

Figure 6a shows the capacitance response curve of the capacitive switch with and without acrylic adhesive liner at different frequency ranges from 0.5 kHz to 10 kHz using the LCR meter. The ΔC decreased non-linearly with the increased applied frequency to the device. Significant changes in ΔC occurred when the switch was induced at low frequency. This implies that the sensitivity is much higher when the applied frequency is low. Compared with the bare capacitive switch, the capacitive switch covered with the acrylic film was characterized by lower changes of ΔC.

However, the changes are still close to those of the bare capacitive switch. Hence, the covering of the acrylic adhesive liner did not affect the performance of the capacitive switch. The advantages of applying the acrylic film are to protect the carbon printed switch, prevent potential damage against sharp fingernails, and ensure the integrity of the printed carbon composite material. In addition, it was found that the capacitive switch responded rapidly during both weak and robust finger tapping (Figure 6b). Moreover, the carbon capacitive sensor was highly responsive to 3 to 4 Hz of finger tapping (fast tapping) compared to slow tapping at 1 Hz (slow tapping), as shown in Figure 6c. The sensitivity of the carbon capacitive switch at 3 to 4 Hz in this work is similar to the sensitivity of the capacitive pressure sensor made of carbon nanotubes/polydimethylsiloxane (CNT/PDMS) at 25 ms reported in [26]. The response time is also shorter than the PS/graphene/MWCNTs tactile sensor at 40 ms [27]. However, the roughness of the abrasive paper as the backing mold must be well controlled to obtain consistent pressure changes at different areas [26]. Comparatively, the switch created in this work does not require the precision of pressure sensing but responsiveness to tapping.

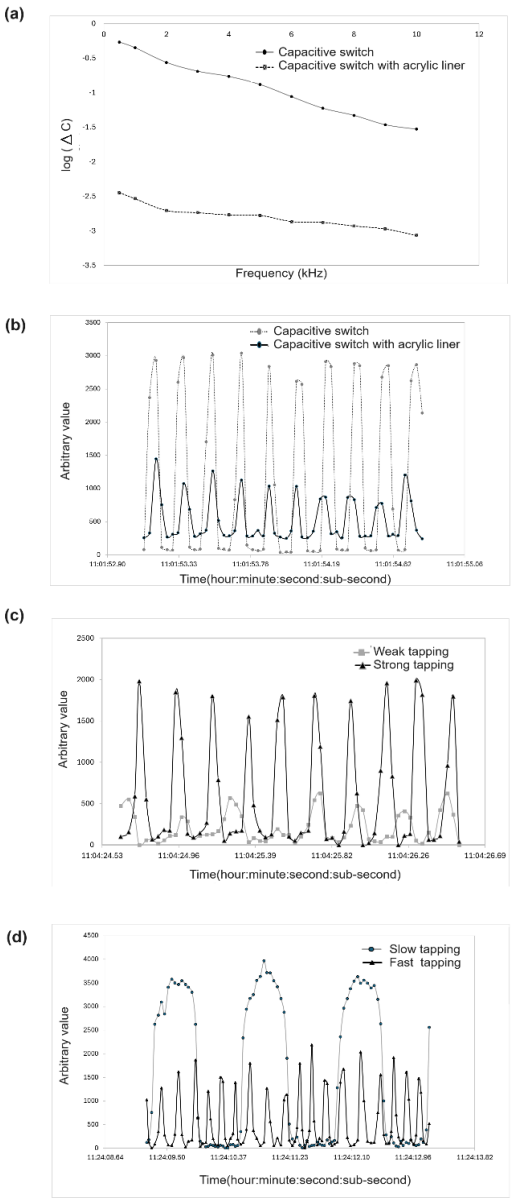

Figure 6. (a) Frequency responses (N=10), (b) time responses at 4 Hz of tapping, and (c) weak/strong tapping of the capacitive switch.

4.0 CONCLUSION

This work reported developing and applying direct writing techniques for rapid, cost-effective prototyping of the capacitive switch. By leveraging direct writing with mini-CNC and extrusion systems, we achieve precise control over the deposition process, enabling the fabrication of complex sensor geometries with high accuracy. The carbon ink reinforced with sodium silicate maintains structural integrity. Moreover, incorporating carbon ink reinforced with sodium silicate ensures compatibility with paper substrates while maintaining structural integrity, providing the durability and longevity of the fabricated switch. The elastic modulus is 3.31±1.3 GPa, and the electrical conductivity range is 100 to 190 S/m. The current conductivity of the linear line of carbon ink was inversely proportional to the length of the carbon ink pattern. The graphite powder was encapsulated in the sodium silicate with an atomic percentage of carbon at 47.4%, as the surface morphology and EDX results implied. The XRD result suggested that the binder did not affect the strong crystallinity of the carbon by including sodium silicate as a reinforcer. The capacitive switch covered with an acrylic adhesive liner displayed sensitivity and maintained a fast

response (3 to 4 Hz) of finger tapping. Through detailed analysis and experimentation of this work, this research successfully demonstrated the application of DIW in printing functional capacitive switches with suitable physical and electrical properties. The findings of this study contributed to the realization of innovative and versatile sensor fabrication solutions.

Acknowledgement

Communication of this research is made possible through monetary assistance from Universiti Tun Hussein Onn Malaysia and the UTHM Publisher's Office via Publication Fund E15216.

Conflicts of Interest

The author(s) declare(s) that there is no conflict of interest regarding the publication of this paper

References

[1] Fekiri, C., C. Kim, H.-C. Kim, J. H. Cho, I. H. Lee. 2022. Multi-material Additive Fabrication of a Carbon Nanotube-Based Flexible Tactile Sensor. *International Journal of Precision Engineering and Manufacturing*. 23(4): 453-458. DOI: https://doi.org/10.1007/s12541-022-00632-3

[2] Hu, X., W. Yang. 2010. Planar capacitive sensors – designs and applications. *Sensor Review.* 30(1): 24-39. DOI: https://doi.org/10.1108/02602281011010772

[3] Tsamis, E. D., J. N. Avaritsiotis. 2005. Design of planar capacitive type sensor for "water content" monitoring in a production line. *Sensors and Actuators A: Physical.* 118(2): 202-211. DOI: https://doi.org/10.1016/j.sna.2004.07.008

[4] Balke, N., M. Gajek, A. K. Tagantsev, L. W. Martin, Y.-H. Chu, R. Ramesh, S. V. Kalinin. 2010. Direct Observation of Capacitor Switching Using Planar Electrodes. *Advanced Functional Materials*. 20(20): 3466-3475. DOI: https://doi.org/doi.org/10.1002/adfm.201000475

[5] Moheimani, R., P. Hosseini, S. Mohammadi, H. Dalir. 2022. Recent Advances on Capacitive Proximity Sensors: From Design and Materials to Creative Applications. *C (Journal of Carbon Research)* 8(2): 26. DOI: https://doi.org/10.3390/c8020026.

[6] Gong, X., K. Huang, Y.-H. Wu, X.-S. Zhang. 2022. Recent progress on screen-printed flexible sensors for human health monitoring. *Sensors and Actuators A: Physical.* 345: 113821. DOI: https://doi.org/10.1016/j.sna.2022.113821

[7] Shim, J.-S., J. A. Rogers, S.-K. Kang. 2021. Physically transient electronic materials and devices. *Materials Science and Engineering: R: Reports.* 145: 100624. DOI: https://doi.org/10.1016/j.mser.2021.100624

[8] Li, Y., B. Li. 2022. Direct ink writing 3D printing of polydimethylsiloxane-based soft and composite materials: a mini review. *Oxford Open Materials Science*. 2(1): itac008. DOI: https://doi.org/10.1093/oxfmat/itac008

[9] Pinargote, N., A. Smirnov, N. Peretyagin, A. Seleznev, P. Peretyagin. 2020. Direct Ink Writing Technology (3D Printing) of Graphene-Based Ceramic Nanocomposites: A Review. *Nanomaterials (Basel)*. 10(7). DOI: https://doi.org/10.3390/nano10071300

[10] Fatimah, S., R. Ragadhita, D. F. A. Husaeni, A. B. D. Nandiyanto. 2022. How to Calculate Crystallite Size from X-Ray Diffraction (XRD) using Scherrer Method. *ASEAN Journal of Science and Engineering*. 2(1). DOI: https://doi.org/10.17509/ajse.v2i1.37647

[11] Saowadee, N., K. Agersted, J. R. Bowen. 2017. Lattice constant measurement from electron backscatter diffraction patterns. *Journal of Microscopy*. 266(2): 200-210. DOI: https://doi.org/10.1111/jmi.12529

[12] Oliver, W. C., G. M. Pharr. 1992. An improved technique for determining hardness and elastic modulus using load and displacement sensing indentation experiments. *Journal of Materials Research.* 7(6): 1564-1583. DOI: https://doi.org/10.1557/JMR.1992.1564

[13] Tsai, J.-L., J.-F. Tu. 2010. Characterizing mechanical properties of graphite using molecular dynamics simulation. *Materials & Design.* 31(1): 194-199. DOI: https://doi.org/10.1016/j.matdes.2009.06.032

[14] Winkler, C., U. Schwarz, J. Konnerth. 2018. Effect of thermal postcuring on the micro- and macromechanical properties of polyurethane for wood bonding. *Applied Adhesion Science*. 6(1): 5. DOI: https://doi.org/10.1186/s40563-018-0106-3

[15] L. Gray, *Electricity in Physical Science.* Gareth Stevens Publishing LLLP: 2011.

[16] Nur Munirah, A., M. R. Anika Zafiah, A. M.F.L. 2015. Synergistic influence of graphite on biopolymer composites properties. *Jurnal Teknologi*. 77(32). DOI: https://doi.org/10.11113/jt.v77.6981

[17] Popova, A. N. 2017. Crystallographic analysis of graphite by X-Ray diffraction. *Coke and Chemistry*, 60(9). DOI: https://doi.org/10.3103/S1068364X17090058

[18] Aguilar-Bolados, H., M. Yazdani-Pedram, A. Contreras-Cid, M. A. López-Manchado, A. May-Pat, F. Avilés. 2017. Influence of the morphology of carbon nanostructures on the piezoresistivity of hybrid natural rubber nanocomposites. *Composites Part B: Engineering*. 109: 147-154. DOI: https://doi.org/10.1016/j.compositesb.2016.10.057

[19] Rachmanto, M. K. A., L. T. Wibowo, T. Paramitha, A. Purwanto. 2021. Evaluation of Anode Composition in Lithium-Ion Batteries. *Journal of Physics: Conference Series*. 1858(1): 012035. DOI: https://doi.org/10.1088/1742-6596/1858/1/012035

[20] Choi, J. S., H.-K. Lee, S. J. An. 2015. Synthesis of a graphene oxide/sodium silicate nanocomposite using sodium silicate solution. *Royal Society of Chemistry Advances*. 5(48): 38742-38747. DOI: https://doi.org/10.1039/C5RA05241F

[21] Kahlenberg, V. 2010. Structural Chemistry of Anhydrous Sodium Silicates–A Review. *CHIMIA*. 64 (10): 716. DOI: https://doi.org/10.2533/chimia.2010.716

[22] Li, Z. Q., C. J. Lu, Z. P. Xia, Y. Zhou, Z. Luo. 2007. X-ray diffraction patterns of graphite and turbostratic carbon. *Carbon*. 45 (8): 1686-1695. DOI: https://doi.org/10.1016/j.carbon.2007.03.038

[23] Barnakov, C. N., G. P. Khokhlova, A. N. Popova, S. A. Sozinov, Z. R. Ismagilov. 2015. XRD Characterization of the Structure of Graphites and Carbon Materials Obtained by the Low-Temperature Graphitization of Coal Tar Pitch. E*urasian Chemico-Technological Journal*. 17(2): 87-93. DOI: https://doi.org/10.18321/ectj198

[24] Salah, N., A. M. Alfawzan, A. Saeed, A. Alshahrie, W. Allafi. 2019. Effective reinforcements for thermoplastics based on carbon nanotubes of oil fly ash. *Scientific Report*. 9(1): 20288. DOI: https://doi.org/10.1038/s41598-019-56777-1.

[25] Thakur, A. S., V. Srivastava, R. Vaish. 2024. Pencil-drawn Interdigitated Capacitive Sensors on Wood Substrate. *Advanced Sensor and Energy Materials*. 100103. DOI: https://doi.org/10.1016/j.asems.2024.100103

[26] Duan, Y., J. Wu, S. He, B. Su, Z. Li, Y. Wang. 2022. Bioinspired Spinosum Capacitive Pressure Sensor Based on CNT/PDMS nanocomposites for Broad Range and High Sensitivity. *Nanomaterials*. 12: 3265. DOI: https://doi.org/ 10.3390/nano12193265.

[27] Qiu, J., X. Guo, R. Chu, S. Wang, W. Zeng, L. Qu, Y. Zhao, F. Yan, G. Xing. 2019. Rapid response, low detection limit, and high sensitivity capacitive flexible tactile sensor based on three-dimensional porous dielectric layer for wearable electronic skin. *ACS Applied Materials & Interfaces* 11(43): 40716–40725. DOI: https://doi.org/10.1021/acsami.9b16511.